Frontiers of Physics
https://doi.org/10.1007/s11467-019-0947-7
Front. Phys.
15(2), 22603 (2020)

RESEARCH ARTICLE

# Optimal spectral phase control of femtosecond laser-induced up-conversion luminescence in $Sm^{3+}$:$NaYF_4$ glass

**Jian-Ping Li[1], Lian-Zhong Deng[1,†], Ye Zheng[1], Peng-Peng Ding[1], Tian-Qing Jia[1], Zhen-Rong Sun[1], Jian-Rong Qiu[2], Shi-An Zhang[1,3,‡]**

[1] *State Key Laboratory of Precision Spectroscopy, School of Physics and Electronic Science, East China Normal University, Shanghai 200062, China*
[2] *State Key Laboratory of Modern Optical Instrumentation, College of Optical Science and Engineering, Zhejiang University, Hangzhou 310027, China*
[3] *Collaborative Innovation Center of Extreme Optics, Shanxi University, Taiyuan 030006, China*
*Corresponding authors. E-mail: †lzdeng@phy.ecnu.edu.cn, ‡sazhang@phy.ecnu.edu.cn*
*Received July 29, 2019; accepted November 6, 2019*

The spectral phase of the femtosecond laser field is an important parameter that affects the up-conversion (UC) luminescence efficiency of dopant lanthanide ions. In this work, we report an experimental study on controlling the UC luminescence efficiency in $Sm^{3+}$:$NaYF_4$ glass by 800-nm femtosecond laser pulse shaping using spectral phase modulation. The optimal phase control strategy efficiently enhances or suppresses the UC luminescence intensity. Based on the laser-power dependence of the UC luminescence intensity and its comparison with the luminescence spectrum under direct 266-nm femtosecond laser irradiation, we propose herein an excitation model combining non-resonant two-photon absorption with resonance-mediated three-photon absorption to explain the experimental observations.

**Keywords** up-conversion luminescence, rare earth ions, quantum control, femtosecond laser, spectral phase

Manipulating the up-conversion (UC) luminescence of lanthanide ion-doped luminescent materials has attracted considerable attention owing to its significant and wide applications. Over the years, a number of schemes have been developed to enhance or control the UC luminescence efficiency of doped lanthanide ions. These goals are often achieved by changing the properties of the luminescent materials, such as varying the lanthanide dopant [1, 2], dopant concentration [3–5], and nanoparticle size [6, 7], preparing a core–shell structure [8–10], and even synthesizing a "native" layer via the high-temperature air annealing process [11]. Another option is modulating the environment around the sample using various means, such as applying an electric or magnetic field [12, 13] or varying the sample temperature [14]. Further, controlling the laser parameters of the excitation source, such as varying the excitation wavelength [15], pulse duration [16], repetition rate [17], or spectral phase [18, 19], is also an efficient way.

Near-infrared lasers have been widely used as the excitation source for UC luminescence generation from doped lanthanide ions because of their important advantages, such as deep tissue penetration, small background spontaneous fluorescence, and reduced risk of light bleaching and damage. Under near-infrared laser excitation, $Sm^{3+}$ ion-doped luminescent materials can emit strong UC luminescence signals in the visible region [20], which have important applications in phosphors [21, 22], laser materials [23], sensors [24] and other optoelectronic devices [25]. Near-infrared femtosecond lasers, which have high peak power and wide spectral bandwidth, are particularly excellent light sources for UC luminescence excitation via non-resonance or resonance-mediated multi-photon absorptions. Spectral phase modulation can be used for femtosecond pulse shaping, which can induce constructive or destructive interference of the multi-photon excitation pathways. In this way, the UC luminescence efficiency can be adjusted.

The co-doping strategy (using dopants such as $Yb^{3+}$/$Er^{3+}$, $Yb^{3+}$/$Ho^{3+}$, or $Yb^{3+}$/$Tm^{3+}$) achieves higher UC luminescence efficiency than the single-doping strategy (using ions such as $Er^{3+}$, $Ho^{3+}$, or $Tm^{3+}$). Nevertheless, we focus on exploring the physical excitation mechanism of single-doped $Sm^{3+}$ irradiated with an 800-nm femtosecond laser pulse. As one of the most widely used substrates, $NaYF_4$ is selected owing to its low phonon energy [26]. There is no intermediate energy level that is corresponding to the single-photon absorption of the 800-nm femtosecond laser for the doping $Sm^{3+}$ ion, Therefore, the most probable absorption from the ground state $^6H_{5/2}$ to the excited state $^6P_{3/2}$ is a non-resonant two-photon process. According to previous studies [27, 28], the absorption probability of a non-resonant two-photon process is max-

© Higher Education Press and Springer-Verlag GmbH Germany, part of Springer Nature 2020

imized under transform-limited laser pulses, and spectral phase modulation of the excitation pulse suppresses rather than enhances the absorption probability. However, we have experimentally observed UC luminescence enhancement under spectral phase modulation. These observations cannot be explained by the conventional excitation model of non-resonant two-photon absorption. Therefore, we propose a new excitation model that combines non-resonant two-photon absorption with resonance-mediated three-photon absorption and support it with experimental proofs. This study can further our understanding of the excitation mechanism of dopant $Sm^{3+}$ ions and will make positive contributions to the related applications of co- or multi-doping strategies.

Figure 1 shows a schematic of the experimental arrangement. A Ti–Sapphire mode-locked regenerative amplifier outputs femtosecond laser pulses with a central wavelength of 800 nm, an approximate pulse duration of 50 fs, and a repetition rate of 1 kHz. The output femtosecond laser pulse is steered into a programmable 4f-configuration zero-dispersion pulse shaper, which comprises a pair of diffraction gratings (1200 lines/mm), a pair of concave mirrors (focal length 200 mm), and a one-dimensional liquid-crystal spatial light modulator (SLM) of 640 pixels. Then, the shaped femtosecond laser pulse is guided through a variable attenuator and a beam splitter and finally focused on the measured sample through a lens with 50-mm focal length. Here, the femtosecond laser intensity irradiating the sample is varied using the attenuator and the beam splitter reflects a small portion of the laser intensity onto a dynamometer, which monitors the femtosecond laser intensity incident on the sample. The fluorescence signals from the sample are measured by a fiber spectrometer with a charge-coupled device in the direction perpendicular to the laser propagation. A PC is used to record the luminescence spectrum and updates the SLM control voltage.

The experimental sample was $Sm^{3+}$:$NaYF_4$ glass comprising 39.5% $SiO_2$, 25% $Al_2O_3$, 18% $Na_2CO_3$, 10% $YF_3$, 7% NaF, and 0.5% Sm (mol%). First, the mixed raw materials are melted into a liquid at 1350°C for approximately 45 min in a platinum crucible at atmospheric pressure. The melted liquid is injected into a metal mold and annealed for 10 h at 450°C. Finally, the obtained glass is properly cut and polished prior to measurement.

Figure 2(a) shows the UV–VIS–NIR absorption spectrum of the $Sm^{3+}$:$NaYF_4$ glass sample. In addition to the strong absorption band in the UV region, an obvious absorption peak appears at approximately 402 nm corresponding to the transition from the ground state $^6H_{5/2}$ to the excited state $^6P_{3/2}$; this is more clearly shown in the inset. Note that no absorption peak appears around 800 nm because there are no corresponding energy levels. Under 800-nm femtosecond laser excitation, the UC luminescence signals in the visible region can be clearly observed [see Fig. 2(b)]. The four distinct emission bands are centered around 563, 599, 647, and 710 nm. Generally, these luminescence peaks are assigned to the state transitions of $^4G_{5/2} \rightarrow {}^6H_{5/2}$, $^4G_{5/2} \rightarrow {}^6H_{7/2}$, $^4G_{5/2} \rightarrow {}^6H_{9/2}$, and $^4G_{5/2} \rightarrow {}^6H_{11/2}$, respectively [29].

The femtosecond laser has a wide spectral bandwidth and can induce many excitation pathways in the UC luminescence generation of rare earth ions. However, the spectral phase distribution of the laser pulse can determine the constructive or destructive interference of these excitation pathways and affect the UC luminescence efficiency. In this work, we use an optimal phase control strategy based on a generic algorithm (GA) to manipulate the UC luminescence intensity. The GA-based adaptive program has been described previously [30]. In our experiment, the luminescence intensity at 599 nm is used as the feedback signal for optimization, and the femtosecond laser intensity is set to approximately $1.6 \times 10^{13}$ W/cm$^2$. As shown in Fig. 3(a), the luminescence intensity can be either efficiently enhanced (red line) to approximately 1.4 times that of the transform-limited laser pulse (black line) or greatly suppressed (blue line) to approximately 5% of its value via phase optimization. The phase masks of the femtosecond laser spectrum under enhancement and suppression are shown in Figs. 3(b) and (c), respectively. The

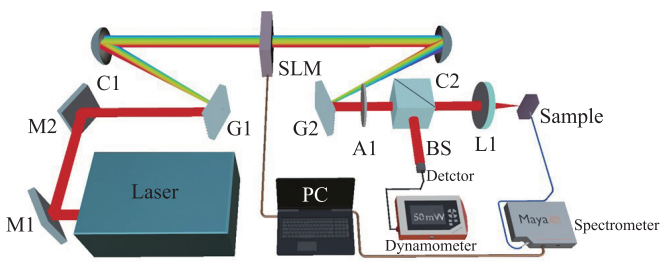



**Fig. 1** Experimental arrangement for manipulating UC luminescence in $Sm^{3+}$:$NaYF_4$ glass by optimally controlling the spectral phase of the femtosecond laser field. SLM: spatial light modulator; C: cylindrical concave mirror; G: grating; L: lens; M: mirror; A: attenuator; BS: beam splitter; PC: personal computer.

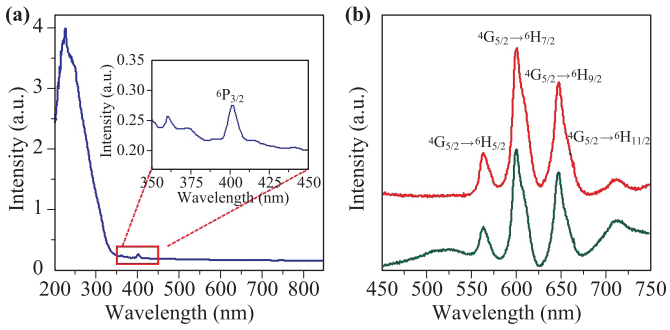



**Fig. 2** UV–VIS–NIR absorption spectra of $Sm^{3+}$:$NaYF_4$ glass **(a)**; luminescence spectra of $Sm^{3+}$:$NaYF_4$ glass under 800- (red line) and 266-nm (cyan line) femtosecond laser excitations **(b)**.

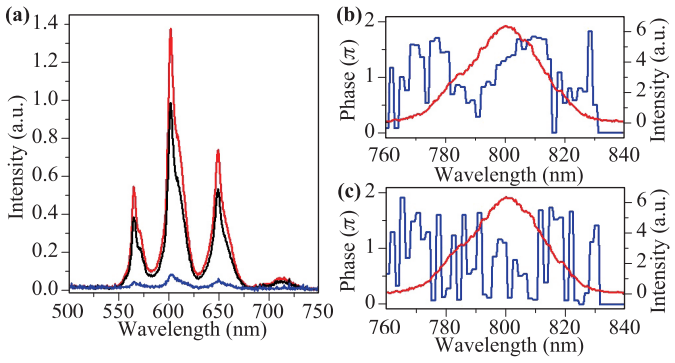



**Fig. 3** **(a)** Luminescence spectra after optimal enhancement (red line) and suppression (blue line) with the original luminescence spectrum (black line). Optimal phase masks (blue) for the femtosecond laser spectrum (red) under UC luminescence enhancement **(b)** and suppression **(c)**, respectively.

spectral phase distribution of the laser pulse was strongly modulated, particularly in the case of luminescence suppression.

The energy level structures of rare earth ions doped in solid substrates are rather complicated. Detailed knowledge of the doping rare earth ions is usually difficult to obtain; therefore, the real experimental situation might be far from the theoretical ideal. Many other factors will make unknown contributions to the experimental results, such as the asymmetry of the femtosecond pulse in the time and frequency domains, mismatch between the central laser frequency and ion resonant frequency, and different phases introduced to various spectral components by the optical elements (e.g., lenses). The GA-based adaptive optimization control adopted herein incorporates all of these influencing factors without any prior knowledge. Depending on the real conditions of the system under study, various phase distributions can be tailored to control and, in particular, suppress the UC luminescence intensity. From the phase masks, direct observation of the excitation mechanisms for luminescence enhancement or suppression is difficult. Consequently, more auxiliary experiments and theoretical analysis are needed.

For the femtosecond laser-induced multi-photon absorption process, the relationship between the luminescence intensity $I$ and pump laser intensity $P$ can be described as $I \propto P^n$, where $n$ is the number of absorbed photons. Figure 4 is a log–log plot showing the laser-intensity dependence of the luminescence intensity at 599 nm. The luminescence intensity increases (initially slow and subsequently fast) with increasing laser intensity within the explored laser intensity range. The experimental data for the low and high laser intensities were linearly fitted with slopes of 1.8 and 2.3, respectively. This experimental observation indicates that two-photon absorption dominates the whole excitation process at low laser intensities but three-photon absorption process might play a role at high laser intensities. To verify the existence of three-photon absorption excitation, we measured the down-conversion (DC) luminescence spectrum of the glass sample under 266-nm femtosecond laser excitation. The experimental result is given in Fig. 2(b) (cyan line). Here, the 266-nm laser is obtained via the third-harmonic generation of an 800-nm laser pulse. As expected, the spectral shape is very similar to that obtained under 800-nm femtosecond laser excitation and the four characteristic luminescence peaks can be clearly observed.

Based on the above studies and the energy level structure of $Sm^{3+}$ [31], we propose the following excitation model to account for the observed luminescence variation under phase-modulated 800-nm femtosecond laser irradiation (see Fig. 5). The population in the ground state $^6H_{5/2}$ is first pumped to the excited state $^6P_{3/2}$ through the simultaneous absorption of two photons. Then, the population in the excited state $^6P_{3/2}$ can decay to the excited state $^4G_{5/2}$ via phonon-assisted relaxation, emitting various fluorescence signals in the visible spectrum [32]. This excitation process, labeled channel ① in Fig. 5, is a non-resonant two-photon absorption process. Moreover, the population in the excited state $^6P_{3/2}$ can be further pumped to the higher excited state $^2H_{9/2}$ through the absorption of a third photon. Similarly, the population in the higher excited state $^2H_{9/2}$ can decay to the

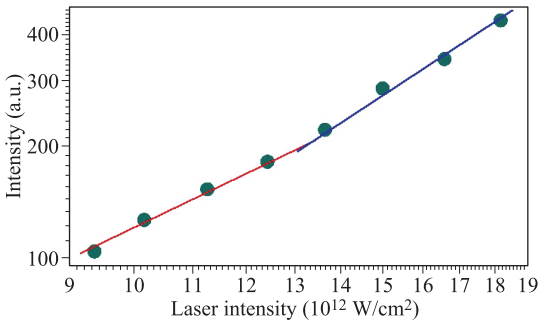



**Fig. 4** Laser-intensity dependence of the luminescence intensity at 599 nm plotted on a log–log scale. The red and blue lines show the linear fittings at low and high laser intensities, respectively.

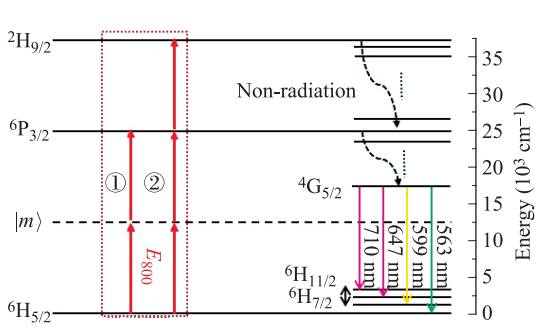



**Fig. 5** Energy level diagram of $Sm^{3+}$ ions and proposed excitation model combining non-resonant two-photon absorption and resonant-mediated three-photon absorption during UC luminescence under 800-nm femtosecond laser excitation.

lower excited state $^4G_{5/2}$ and the same fluorescence signals are emitted. This excitation process is a resonance-mediated $(2+1)$ three-photon absorption and labeled as channel ②. In addition, the population in the ground state $^6H_{5/2}$ can be directly excited to the higher excited state $^2H_{9/2}$ by simultaneously absorbing three photons without via the intermediate state $^6P_{3/2}$; this is called direct non-resonant three-photon absorption. As we know, compared with the resonance-mediated $(2+1)$ three-photon absorption, direct non-resonant three-photon absorption has significantly lower transition probability. Previous studies have confirmed that the transition probability of a non-resonant three-photon excitation can only be suppressed by spectral phase modulation [28]; however, the transition probability of the resonance-mediated (2+1) three-photon absorption can be either enhanced or suppressed, depending on the spectral phase distribution [33]. Based on the aforementioned analysis, we expect that the resonance-mediated $(2+1)$ three-photon absorption should play a much considerably more important role than the direct non-resonant three-photon absorption for the UC luminescence excitation in our case.

In the excitation model shown in Fig. 5, the total transition probability $P^{(T)}$ of $Sm^{3+}$ ions under 800-nm femtosecond laser excitation is given by

$$P^{(T)} = P^{(2)} + P^{(2+1)}, \tag{1}$$

where $P^{(2)}$ and $P^{(2+1)}$ are the transition probabilities of non-resonant two-photon absorption and resonance-mediated $(2+1)$ three-photon absorption, respectively. For convenience of description, the symbols of $|g\rangle$, $|i\rangle$, and $|f\rangle$ are used to represent the ground state $^6H_{5/2}$, intermediate excited state $^6P_{3/2}$, and final excited state $^2H_{9/2}$, respectively. Here, the transition probability $P^{(2)}$ can be calculated as follows:

$$P^{(2)} = \int_{-\infty}^{\infty} g(\omega_i)|a_i^{(2)}|^2 \mathrm{d}\omega_i, \tag{2}$$

with

$$a_i^{(2)} = -\frac{1}{\mathrm{i}\hbar^2}\mu_{ig}^2 A^{(2)}(\omega_i), \tag{3}$$

$$A^{(2)}(\Omega) = \int_{-\infty}^{\infty} E(\omega)E(\Omega-\omega)\mathrm{d}\omega. \tag{4}$$

Here, $a_i^{(2)}$ represents the transition amplitude from state $|g\rangle$ to state $|i\rangle$ via non-resonant two-photon absorption, $\mu_{ig}^2$ is the effective non-resonant two-photon dipole coupling from state $|i\rangle$ to state $|g\rangle$, $g(\omega_i)$ is the absorption line-shape function of state $|i\rangle$, $\omega_i$ is the corresponding transition frequency, and $E(\omega) = E_0(\omega)\exp[\mathrm{i}\Phi(\omega)]$, where $E_0(\omega)$ and $\Phi(\omega)$ are the spectral amplitude and phase, respectively. The transition probability $P^{(2+1)}$ can be obtained as follows:

$$P^{(2+1)} = \int_{-\infty}^{\infty} g(\omega_f)|a_f^{(2+1)}|^2 \mathrm{d}\omega_f, \tag{5}$$

with

$$a_f^{(2+1)} = \frac{1}{\sqrt{2\pi}\hbar^3}\mu_{fi}\mu_{ig}^2\left[\mathrm{i}\pi\int_{-\infty}^{\infty} g(\omega_i)A^{(2)}(\omega_i)E(\omega_f-\omega_i)\mathrm{d}\omega_i + \wp\int_{-\infty}^{\infty} A^{(2)}(\omega_i-\Delta)E(\omega_f-\omega_i+\Delta)\mathrm{d}\Delta/\Delta\right]. \tag{6}$$

Here, $a_f^{(2+1)}$ represents the transition amplitude from states $|g\rangle$ to $|f\rangle$ via resonance-mediated $(2+1)$ three-photon absorption, $\mu_{fi}$ is the dipole matrix element from state $|f\rangle$ to state $|i\rangle$, $g(\omega_f)$ is the absorption line-shape function of the state $|f\rangle$, and $\omega_f$ is the corresponding transition frequency. The first term within bracket in Eq. (6), called the on-resonance term, represents the contributions of all three-photon excitation pathways from the states $|g\rangle$ to $|f\rangle$ that are in resonance with state $|i\rangle$. The second term within brackets in Eq. (6), called the near-resonance term, represents the contributions of all the complementary three-photon excitation pathways in near resonance with state $|i\rangle$, where $\Delta$ is the frequency detuning. The on-resonance pathways (i.e., $\Delta = 0$) are excluded from the near-resonance term by the Cauchy's principal-value operator $\wp$.

As shown in Eqs. (2)–(4), for non-resonant two-photon absorption, the transition probability $P^{(2)}$ can be suppressed but not enhanced by modulating the laser spectral phase. As shown in Eqs. (5) and (6) for the resonance-mediated $(2+1)$ three-photon absorption, the on-resonance term within brackets in Eq. (6) cannot be enhanced. The near-resonance term within brackets in Eq. (6) integrates over both positive ($\Delta > 0$) and negative ($\Delta < 0$) components; therefore, destructive interference is induced by the transform-limited femtosecond laser pulse. A feasible way to enhance the near-resonance contribution is to induce constructive interference instead of destructive interference via spectral phase modulation.

In summary, we have experimentally studied the control of the UC luminescence intensity in the $Sm^{3+}$-ion-doped $NaYF_4$ glass by phase shaping the 800-nm femtosecond excitation laser. The UC luminescence intensity was enhanced or suppressed by adaptively optimizing the spectral phases of the femtosecond laser field. After measuring the laser-power dependence of the UC luminescence intensity and comparing it with the luminescence spectrum of 266-nm femtosecond laser excitation, we proposed an excitation model by combining non-resonant two-photon absorption and resonance-mediated $(2+1)$ three-photon absorption; this was done to account for the experimental observations under phase shaping. Our work provides new insights into the excitation mechanism of dopant $Sm^{3+}$ ions under femtosecond laser irradiation and is potentially valuable for developing related applications.

**Acknowledgements** This work was partly supported by the National Natural Science Foundation of China (Grant Nos. 91850202, 11774094, 11727810, 11804097, and 61720106009), the Science

and Technology Commission of Shanghai Municipality (Grant No. 17ZR146900), the China Postdoctoral Science Foundation (Grant No. 2018M641958), and ECNU Academic Innovation Promotion Program for Excellent Doctoral Students (Grant No. YBNLTS2019-011).

## References

1. S. Y. Han, R. R. Deng, X. J. Xie, and X. G. Liu, Enhancing luminescence in lanthanide-doped upconversion nanoparticles, *Angew. Chem. Int. Ed.* 53(44), 11702 (2014)
2. S. Heer, K. Kömpe, H. U. Güdel, and M. Haase, Highly efficient multicolour upconversion emission in transparent colloids of lanthanide-doped $NaYF_4$ nanocrystals, *Adv. Mater.* 16(23–24), 2102 (2004)
3. F. Wang and X. G. Liu, Upconversion multicolor fine-tuning: Visible to near-infrared emission from lanthanide-doped $NaYF_4$ nanoparticles, *J. Am. Chem. Soc.* 130(17), 5642 (2008)
4. S. H. Wen, J. J. Zhou, K. Z. Zheng, A. Bednarkiewicz, X. G. Liu, and D. Y. Jin, Advances in highly doped upconversion nanoparticles, *Nat. Commun.* 9(1), 2415 (2018)
5. F. Wang and X. G. Liu, Multicolor tuning of lanthanide-doped nanoparticles by single wavelength excitation, *Acc. Chem. Res.* 47(4), 1378 (2014)
6. K. Patel, V. Blair, J. Douglas, Q. L. Dai, Y. H. Liu, S. Q. Ren, and R. Brennan, Structural effects of lanthanide dopants on alumina, *Sci. Rep.* 7(1), 39946 (2017)
7. D. K. Xu, A. M. Li, L. Yao, H. Lin, S. H. Yang, and Y. L. Zhang, Lanthanide-doped $KLu_2F_7$ nanoparticles with high upconversion luminescence performance: A comparative study by Judd-Ofelt analysis and energy transfer mechanistic investigation, *Sci. Rep.* 7(1), 43189 (2017)
8. Q. Shao, Z. Yang, G. Zhang, Y. Hu, Y. Dong, and J. Jiang, Multifunctional lanthanide-doped core/shell nanoparticles: Integration of upconversion luminescence, temperature sensing, and photothermal conversion properties, *ACS Omega* 3(1), 188 (2018)
9. F. Xu, Y. Zhao, M. Hu, P. Zhang, N. Kong, R. Liu, C. Liu, and S. K. Choi, Lanthanide-doped core–shell nanoparticles as a multimodality platform for imaging and photodynamic therapy, *Chem. Commun.* 54(68), 9525 (2018)
10. X. Chen, D. Peng, Q. Ju, and F. Wang, Photon upconversion in core–shell nanoparticles, *Chem. Soc. Rev.* 44(6), 1318 (2015)
11. L. Tian, Y. Shang, S. Hao, Q. Han, T. Chen, W. Lv, and C. Yang, Constructing a "native" oxyfluoride layer on fluoride particles for enhanced upconversion luminescence, *Adv. Funct. Mater.* 28(48), 1803946 (2018)
12. X. Tian, Z. Wu, Y. Jia, J. Chen, R. K. Zheng, Y. Zhang, and H. Luo, Remanent-polarization-induced enhancement of photoluminescence in $Pr^{3+}$-doped lead-free ferroelectric $(Bi_{0.5}Na_{0.5})\,TiO_3$ ceramic, *Appl. Phys. Lett.* 102(4), 042907 (2013)
13. V. K. Tikhomirov, L. F. Chibotaru, D. Saurel, P. Gredin, M. Mortier, and V. V. Moshchalkov, $Er^{3+}$-doped nanoparticles for optical detection of magnetic field, *Nano Lett.* 9(2), 721 (2009)
14. F. Vetrone, R. Naccache, A. Zamarrón, A. Juarranz de la Fuente, F. Sanz-Rodríguez, L. Martinez Maestro, E. Martín Rodriguez, D. Jaque, J. García Solé, and J. A. Capobianco, Temperature sensing using fluorescent nanothermometers, *ACS Nano* 4(6), 3254 (2010)
15. Z. Chen, G. Wu, H. Jia, K. Sharafudeen, W. Dai, X. Zhang, S. Zeng, J. Liu, R. Wei, S. Lv, G. Dong, and J. Qiu, Improved up-conversion luminescence from $Er^{3+}$:$LaF_3$ nanocrystals embedded in oxyfluoride glass ceramics via simultaneous triwavelength excitation, *J. Phys. Chem. C* 119(42), 24056 (2015)
16. C. F. Gainer, G. S. Joshua, C. R. De Silva, and M. Romanowski, Control of green and red upconversion in $NaYF_4$:$Yb^{3+}$, $Er^{3+}$ nanoparticles by excitation modulation, *J. Mater. Chem.* 21(46), 18530 (2011)
17. C. F. Gainer, G. S. Joshua, and M. Romanowski, Toward the use of two-color emission control in upconverting $NaYF_4$: $Er^{3+}$, $Yb^{3+}$ nanoparticles for biomedical imaging, *Nanoscale* 8231, 82310I (2012)
18. S. Zhang, S. Xu, J. Ding, C. Lu, T. Jia, J. Qiu, and Z. Sun, Single and two-photon fluorescence control of $Er^{3+}$ ions by phase-shaped femtosecond laser pulse, *Appl. Phys. Lett.* 104(1), 014101 (2014)
19. P. Liu, W. Cheng, Y. Yao, C. Xu, Y. Zheng, L. Deng, T. Jia, J. Qiu, Z. Sun, and S. Zhang, Observing quantum control of up-conversion luminescence in $Dy^{3+}$ ion doped glass from weak to intermediate shaped femtosecond laser fields, *Laser Phys. Lett.* 14(11), 115301 (2017)
20. E. De la Rosa, L. A. Diaz-Torres, P. Salas, and R. A. Rodriguez, Visible light emission under UV and IR excitation of rare earth doped $ZrO_2$ nanophosphor, *Opt. Mater.* 27(7), 1320 (2005)
21. T. P. Tang, C. M. Lee, and F. C. Yen, The photoluminescence of $SrAl_2O_4$: Sm phosphors, *Ceram. Int.* 32(6), 665 (2006)
22. G. B. Nair and S. J. Dhoble, Photoluminescence properties of $Eu^{3+}/Sm^{3+}$ activated $CaZr_4(PO_4)_6$ phosphors, *J. Fluoresc.* 26(5), 1865 (2016)
23. D. T. Marzahl, P. W. Metz, C. Kränkel, and G. Huber, Spectroscopy and laser operation of $Sm^{3+}$-doped lithium lutetium tetrafluoride ($LiLuF_4$) and strontium hexaaluminate ($SrAl_{12}O_{19}$), *Opt. Express* 23(16), 21118 (2015)
24. J. Liu and Y. K. Vohra, Sm:YAG optical pressure sensor to 180 GPa: Calibration and structural disorder, *Appl. Phys. Lett.* 64(25), 3386 (1994)
25. M. Dyrba, P. T. Miclea, and S. Schweizer, Spectral down-conversion in Sm-doped borate glasses for photovoltaic applications, *Proc. SPIE* 7725, 77251D (2010)
26. J. F. Suyver, J. Grimm, M. K. Van Veen, D. Biner, K. W. Krämer, and H. U. Güdel, Upconversion spectroscopy and properties of $NaYF_4$ doped with $Er^{3+}$, $Tm^{3+}$ and/or $Yb^{3+}$, *J. Lumin.* 117(1), 1 (2006)

27. D. Meshulach and Y. Silberberg, Coherent quantum control of two-photon transitions by a femtosecond laser pulse, *Nature* 396(6708), 239 (1998)

28. D. Meshulach and Y. Silberberg, Coherent quantum control of multiphoton transitions by shaped ultrashort optical pulses, *Phys. Rev. A* 60(2), 1287 (1999)

29. L. Wu, M. Ji, H. Wang, Y. Kong, and Y. Zhang, Site occupancy and photoluminescence of $Sm^{3+}$ in $KSr_4(BO_3)_3$: $Sm^{3+}$ phosphors, *Opt. Mater. Express* 4(8), 1535 (2014)

30. L. Z. Deng, Y. Yao, L. Deng, H. Jia, Y. Zheng, C. Xu, J. Li, T. Jia, J. Qiu, Z. Sun, and S. Zhang, Tuning upconversion luminescence in $Er^{3+}$-doped glass ceramic by phase-shaped femtosecond laser field with optimal feedback control, *Front. Phys.* 14(1), 13602 (2019)

31. W. T. Carnall, P. R. Fields, and K. Rajnak, Electronic energy levels in the trivalent lanthanide aquo ions (I): $Pr^{3+}$, $Nd^{3+}$, $Pm^{3+}$, $Sm^{3+}$, $Dy^{3+}$, $Ho^{3+}$, $Er^{3+}$, and $Tm^{3+}$, *J. Chem. Phys.* 49(10), 4424 (1968)

32. S. Q. Mawlud, M. M. Ameen, M. R. Sahar, Z. A. S. Mahraz, and K. F. Ahmed, Spectroscopic properties of $Sm^{3+}$ doped sodium-tellurite glasses: Judd–Ofelt analysis, *Opt. Mater.* 69, 318 (2017)

33. A. Gandman, L. Chuntonov, L. Rybak, and Z. Amitay, Coherent phase control of resonance-mediated (2 + 1) three-photon absorption, *Phys. Rev. A* 75(3), 031401 (2007)